Chai *et al. Geoenvironmental Disasters* (2024) 11:16
https://doi.org/10.1186/s40677-024-00276-7

Geoenvironmental Disasters

RESEARCH Open Access

Assessment of immediate and five-year earthquake impacts on river systems in sabah, Malaysia using multi-temporal satellite imageries

Lee Ting Chai[1], Anand Nainar[1], Rodeano Roslee[2,3], Wilson Vun Chiong Wong[1] and Mui-How Phua[1*]

Abstract

Background Earthquake is one of the most destructive natural disasters, which cause immediate and long-term changes to the river systems. This research aimed to examine the immediate and five-year impacts of the 2015 Ranau Earthquake (6.0 Mw) on river systems in Malaysian state of Sabah, a region of low earthquake hazard.

Methods We used object-based classification on Landsat 8 (2014 and 2015) and Sentinel-2A (2020) satellite imageries to derive land cover time series for investigating the impacts on the riparian areas.

Results The earthquake removed vegetation in the riparian zones of four rivers, the highest being the Penataran River (69.21 ha). During the immediate impact period (2014–2015), river bar formation occurred in all rivers, with the largest increase occurring in the Kadamaian River (56.97 ha), followed by the Panataran River (54.36 ha), which had no river bar before the earthquake. The river bar of the Kadamaian River continued to increase, whereas the river bar of the Panataran River decreased five years after the earthquake. Land cover transition analysis revealed that 78.39 ha of vegetation, barren land, and river water areas changed to river bars in the Kadamaian riparian area during the immediate impact period. Except for 26.87% of river bars in the Kadamaian riparian area in 2015, most river bars transitioned to other land cover types five years later. During the period of immediate impact, 22.05 ha of vegetation and 10.71 ha of river water were transformed into river bars along the Penataran River. Five years later, except for 16.2 ha, all river bar areas had transitioned to other cover types. Additionally, 17.7 ha of new river bars were formed. This study provides crucial data on post-earthquake land cover changes, particularly river bar formation and changes, for assessing the earthquake impacts on the river systems and supporting impact mitigation.

Keywords Earthquake, Post-earthquake impacts, Land cover transition, Object-based classification

*Correspondence:
Mui-How Phua
pmh@ums.edu.my
[1]Faculty of Tropical Forestry, Universiti Malaysia Sabah, Jalan UMS, Kota Kinabalu, Sabah 88400, Malaysia
[2]Faculty of Science and Natural Resources, Universiti Malaysia Sabah, Jalan UMS, Kota Kinabalu, Sabah 88400, Malaysia
[3]Natural Disaster Research Centre (NDRC), Universiti Malaysia Sabah, Jalan UMS, Kota Kinabalu, Sabah 88400, Malaysia

Introduction

Earthquakes are among the most destructive natural disasters. Strong vibrations during an earthquake cause ground fissures or fractures. Depending on spatial proximity to the fissures, the acceleration and strain in different directions can cause irreversible damage to man-made structures, such as tunnels (Liu et al. 2019). A strong earthquake could trigger large-scale landslides, causing significant natural environmental changes (Ansari et al. 2016). Besides the earthquake's intensity, magnitude, and focal depth, landslides depend mainly on the geology and local topography. Steep slopes with unstable rock formations are more susceptible to earthquake-triggered landslides that deposit massive amounts of sediment and debris in river systems (Basharat et al. 2021; Mahmood et al. 2015). This sudden influx of material may cause flooding and alter the river's morphology by accelerating erosion and altering the geometry of the channel. Complicating matters, these are all additional factors to the naturally occurring drivers of mass movement, namely climate, weathering, streamflow, and other characteristics such as soil type, vegetation, and land-cover that influence geomorphological changes in an area (Nainar et al. 2017; Sidle et al. 2006). Nevertheless, Xue et al. (2013) discovered that significant mass movements were governed by episodic seismic events rather than these recurrent factors. In addition to the immediate effects on river geometry, there have been reports of long-term land cover changes due to accelerated erosion and deposition (Balamurugan and Aravind 2015; Ishihara and Tadono 2017; Rojas et al. 2013; Wang et al. 2022).

Mapping of land cover changes due to a destructive earthquake is crucial for post-earthquake land use planning and management. Satellite remote sensing, particularly medium-resolution satellite sensors, is a highly effective technology for monitoring the state of the earth's surface because of its capacity to provide consistent and high-quality satellite data that repeatedly covers a large area. Medium-resolution imageries such as Landsat data have been effectively used to quantify land cover changes in the aftermath of earthquakes such as the 2001 Gujarat Earthquake (Balamurugan and Aravind 2015), the 2011 Tohoku Earthquake (Ishihara and Tadono 2017), and the 2015 Nepal Earthquake (Fan et al. 2019). Despite the fact that it is essential to analyze the dynamics of land cover and river channel changes for ecosystem restoration, the vast majority of studies only address the overwhelming immediate impact of catastrophic earthquakes (Fan et al. 2019; Ishihara and Tadono 2017).

Land cover changes can be detected and monitored via spectral change analysis or post-classification comparison analysis. Spectral change detection examines the physical changes between imageries related to the spectral signature of the land surface, whereas post-classification (map-to-map) comparison compares multi-temporal satellite maps with an overall accuracy equal to the product of the individual accuracies (Phua et al. 2007). The post-classification comparison method is prevalent because it permits monitoring of the land cover trajectory over the change period (Kamlisa and Bürger-Arndt 2016). This method classifies satellite time series using pixel-based or object-based classification approaches. Pixel-based classification analyses the spectral information of individual image pixels, whereas object-based image analysis aggregates image pixels into spectrally homogeneous segments of image objects by user-defined parameters, such as scale parameter, compactness, and shape, and then classifies the individual image objects (Liu and Xia 2010). Object-based Image Analysis (OBIA) incorporates spatial, textural, and neighborhood relations in classification, which significantly reduces the "salt and pepper" effect associated with the pixel-based approach (Blaschke 2010; Yu et al. 2016; Zhou et al. 2008). Several comparative studies concluded that the object-based classification approach is superior to the pixel-based approach (Li et al. 2016; Phua and Tsuyuki 2021).

The recent integration of deep learning with OBIA represents a significant advancement in satellite image classification (Guirado et al. 2021; Liu et al. 2021; Timilsina et al. 2020). Employing deep learning alongside OBIA requires data transformation to specific data structures for training deep learning models. The needs of extensive computation and hardware capacity (Vali et al. 2020) and a large training dataset to capture different in-class variations (Azeez et al. 2022) could prevent its operational use in monitoring post-earthquake land cover changes. OBIA with deep learning models has shown good performance with high-resolution satellite imageries (Timilsina et al. 2020). However, the spatial resolution of moderate-resolution satellite imageries may be insufficient for the classifier (Vali et al. 2020).

Sabah, located in the northern portion of Borneo, has a low earthquake hazard because it is located far from major plate boundary faults (Wang et al. 2017). Active faults, including thrust faults, strike-slip faults, and normal faults, are associated with earthquakes in Sabah (Tjia 1978, 2007; Tongkul 1989, 2017; Wang et al. 2017). According to the USGS earthquake database, approximately 67 low- to moderate-magnitude earthquakes were recorded onshore and offshore Sabah from 1900 to 2019. Most of Sabah's earthquakes with magnitudes below 5.0 Mw were in Ranau and Lahad Datu (Tongkul 2021). On June 5, 2015, Ranau was shaken by a 6.0 Mw earthquake. This seismic event continued for approximately 30 s. It was detectable as far as 400 km from the epicentre, which, situated nearly 10 km deep, was the most significant earthquake in Malaysia since the Mw 6.2 Lahad Datu earthquake in 1976 (Adnan and Harith 2017;

Tongkul 2016). According to Rosli et al. (2021), the primary hazard of the earthquake involved direct geological failures, which was observed at the foot slope of Mount Kinabalu, the tallest mountain in the region and the centrepiece of Kinabalu Park (UNESCO World Heritage Site. Widespread rockfalls and numerous landslides were triggered by the mainshock and a series of aftershocks near Mount Kinabalu, forming a temporary landslide dam. The secondary hazard identified as debris flow occurred along the river channels. Rosli et al. (2021) reported two debris flows, i.e. the Mesilau watershed of Kundasang on the Southeast flank of Mount Kinabalu and the Kadamaian watershed of Kota Belud, located on the northwest flank of Kota Belud. A significant debris flow in the Mount Kinabalu area on June 13, 2015, led to the deposition of large amounts of mud and loose boulders along the river channels (Sharir et al. 2022).

As a result, significant amounts of enormous boulders, rocks, gravel, and sand were transported and deposited along the river channel, forming river bars, particularly in the downstream areas of the Kota Belud district. River bars are elevated but shallow sections of the riverbed's topography that are created by sediment deposition. River bars are visible during periods of low flow and can be migratory or stationary (Wright and Crosato 2011). According to Croissant et al. (2019), debris left on hillslopes after earthquakes is only expected to remain stationary for a brief period. Although the 2015 Ranau earthquake has substantially altered river systems in the Kota Belud district, the impacts have not been quantified. Using multi-temporal satellite imageries, our study aimed to investigate the earthquake-induced land cover changes in the impacted river systems of the Kota Belud district. The OBIA was used to classify satellite imageries of pre-earthquake, immediate (approximately 1 year), and five-year impacts. We analyzed and compared the changes in land cover caused by earthquakes in the riparian areas of five rivers in order to identify the rivers with the greatest impact. Further land cover transition analyses of river bars in these rivers were performed to determine the immediate and five-year impacts.

Materials and methods

Study area

Sabah is located in the northern part of Borneo Island, on the Eurasian Plate (Fig. 1). The study area is located

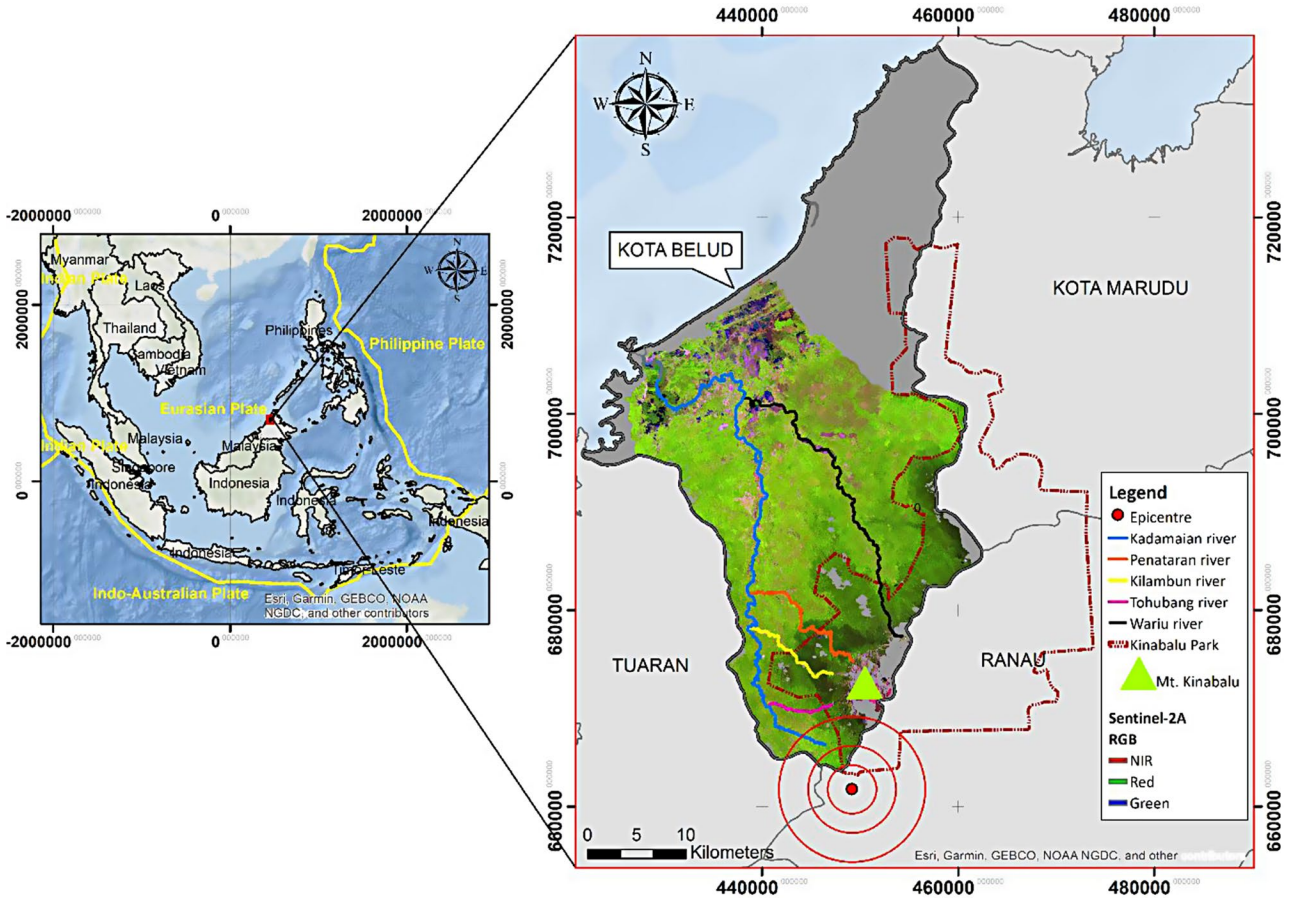

Fig. 1 Location of the study area, Kota Belud, Sabah, Malaysia

in Kota Belud district (WGS 1984 UTM Zone 50 N 436,725 m E 702,289 m N), Sabah, Malaysia. Kota Belud has an area of approximately 1,386 km^2. The climate is equatorial, with high temperatures and abundant rainfall all year round. The adjacent weather station shows a daily temperature between 32.2 °C and 44.3 °C and a mean annual precipitation of 2,547.2 mm (World Weather Information Service, 2010). The study area is influenced by the northeast (November-March) and southwest (late May-September) monsoons. The northeast monsoon brings heavy rainfall and strong winds, though the effects are less severe on the west coast. The southwest monsoon is characterised by lower humidity and rainfall in the west coast. Inter-monsoon periods have relatively calm winds with frequent thunderstorms in the afternoon. The elevation within the district ranges from close to sea level to over 4000 m above sea level. The topography of these high-elevation areas is typically rugged, comprising steep hillslopes and deep valleys. Mount Kinabalu, at 4,095.2 m, is the highest mountain between the Himalayas and New Guinea. This mountain is located in Kinabalu Park (75,370 ha), a World Heritage Site. Five rivers in Kota Belud, namely the Wariu River, Penataran River, Kilambun River, Tohubang River, and Kadamaian River, originate from Mount Kinabalu (Fig. 2).

Pre-processing of multi-temporal satellite imageries

Two imageries of Landsat 8 Operational Land Imager (OLI) (April 2014 and October 2015) and imagery of Sentinel-2 A Multispectral Instrument (MSI) (August 2020) were acquired from the United States Geological Service (USGS) Earth Explorer (http://earthexplorer.usgs.gov) to analyze the earthquake-induced land cover changes in one-year (immediate impact) and five-year (five-year impact) change periods. Radiometric correction included converting a digital number (DN) to top-of-atmosphere (TOA) reflectance and removing atmospheric and topographic effects. All imageries were georeferenced to the same map projection system (Universal Transverse Mercator Zone 50 N). These satellite imageries were contaminated by clouds to varying degrees, so multiple scenes from the same year were downloaded and mosaicked to create a cloud-free or nearly cloud-free image in ArcGIS for each year. The watersheds of five rivers (Wariu River, Kadamaian River, Penataran River, Kilambun River and Tohubang River) were generated using the Shuttle Radar Topography Mission (SRTM) Digital Elevation Model (DEM) and combined as the study area polygon, which was used to extract the multi-temporal satellite imageries for object-based land cover classification.

Object-based land cover classification and change detection

Object-based classification effectively reduces misclassification due to within-class variations and minimizes the "salt and pepper" effect (Phiri and Morgenroth 2017). Landsat and Sentinel-2 imageries were analyzed with OBIA in eCognition Developer software (Trimble Inc.). The OBIA involves image segmentation, followed by the selection of training samples and classification. Multiresolution segmentation was used in this study. The segmentation outcome depends on three main factors: (i)

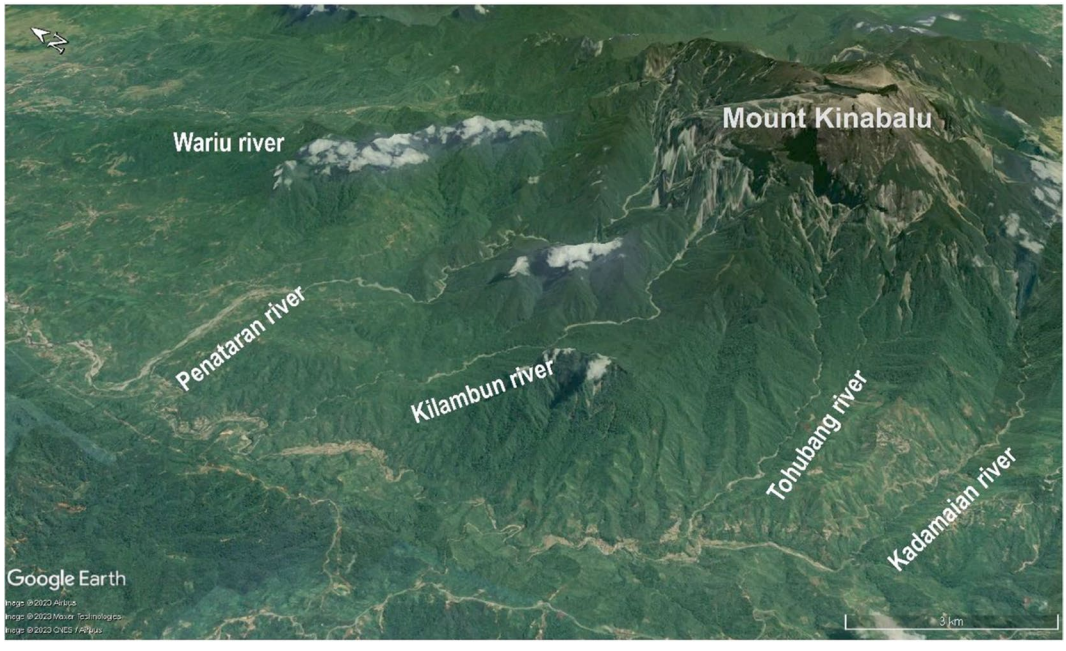

Fig. 2 Main rivers in the Kota Belud district

Table 1 The optimal scale and parameters during image segmentation

Parameters	Level 1 Segmentation		Level 2 Segmentation	
	Landsat 8	Sentinel-2	Landsat 8	Sentinel-2
Scale	1.0	2.0	0.3	0.6
Shape/ Color	0.0001/ 0.9999		0.0001/ 0.9999	
Compactness/ Smoothness	0.4/ 0.6		0.4/ 0.6	

the homogeneity criterion or scale parameter that determines the maximum allowed heterogeneity for the resulting segments; (ii) the weight of color and shape criteria in the segmentation process (shape); and (iii) the weight of the compactness and smoothness criteria (compactness) (Aguilar et al. 2016).

Large-scale parameter values result in delineating big objects with high spectral variations. First, we visually inspected the segmentation results of different scale parameters to determine the suitable scale parameter value. Next, we conducted testing of different combinations of shapes and compactness weights between 0 and 1. Increasing the shape parameter value lowers the influence of the color parameter in segmentation. The image objects will be more compact by increasing the compactness parameter value. We iteratively determined the combination of scale, shape, and compactness parameters by visual assessment (Table 1). Level 1 segmentation distinguished vegetation and non-vegetation covers and produced larger objects, while Level 2 generated finer objects for classification (Fig. 3). Training samples were selected for each land cover class to train the nearest neighbor classifier in the eCognition software. Object features used by the classifier to classify the image objects included the mean reflectance value of the spectral bands, the Normalized Difference Vegetation Index (NDVI), and the Normalized Difference Water Index (NDWI). We classified the satellite imageries into four land cover classes: Vegetation, Barren Land, River water and River Bar (Fig. 4).

Accuracy assessment compares the classified land covers to the actual land covers. We collected 200 reference points in the field and interpreted orthophotos acquired using a UAS to assess land cover classification accuracy. Google Earth high-resolution imageries were also used to check for any changes at these point locations. We computed the user, producer, and overall accuracies based on the error matrix. Besides, Cohen's kappa (k) coefficient of the agreement was calculated. It may range from −1 to 1, with 1 indicating perfect agreement between the predicted and actual land cover classes and vice versa.

The riparian area (50 m from the river) was derived using buffer analysis in ArcGIS software. The riparian zone of the Kadamaian River was the largest among the five, consisting of 1,358 ha or 58.74% of the total riparian area (2,312 ha). It was followed by the Wariu River (428 ha or 18.51%), Penataran River (264 ha or 11.42%), Kilambun River (177 ha or 7.66%) and Tohubang River (85 ha or 3.68%). These riparian polygons were used to extract the land cover classifications for analyzing the changes. Land cover classification pairs of consecutive

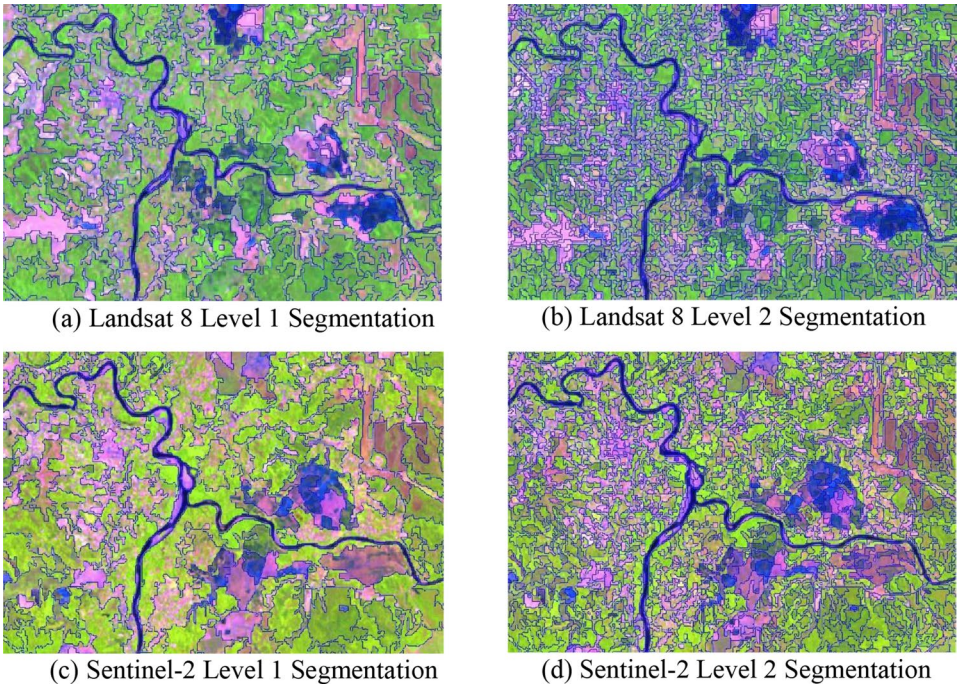

Fig. 3 Segmentation of Landsat 8 imageries (**a**, **b**) and Sentinel-2 imagery (**c**, **d**)

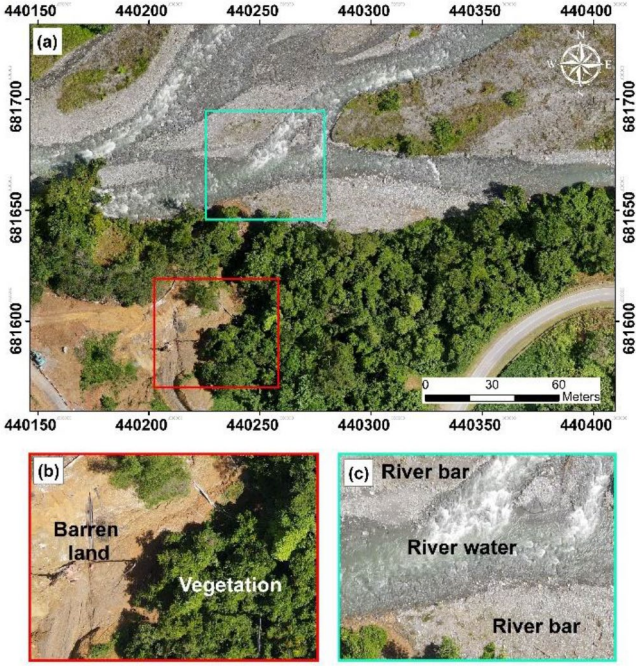

Fig. 4 (**a**) Unmanned Aerial System (UAS) Orthophoto of Penataran River after the earthquake, (**b**) Red box shows the barren land and vegetation classes, and (**c**) Cyan box shows river water and river bar classes

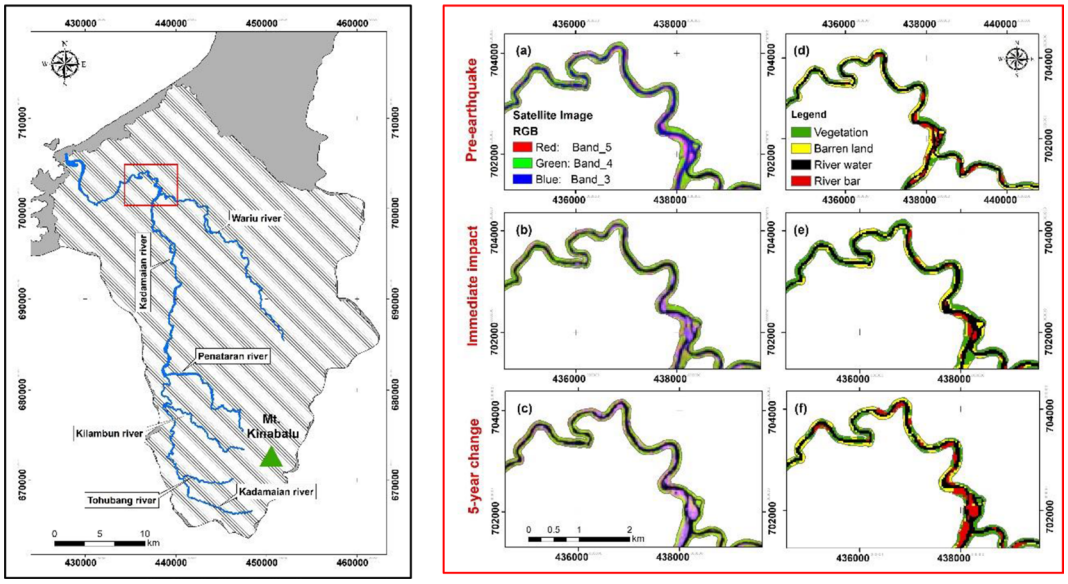

Fig. 5 Landsat 8 false-color composites of 2014 and 2015 (**a**, **b**); Sentinel-2A false-color composite of 2020 (**c**). Object-based land cover classifications of a section of riparian area for 2014, 2015 and 2020 (**d**–**f**)

years were cross-tabulated to investigate land cover changes from 2014 to 2015 (immediate impact) and 2015 to 2020 (five-year impact).

Results

Land cover classifications and accuracies

Figure 5 shows the land cover classifications extracted using the riparian polygons. The error matrices of the land cover classifications are compiled in Table 2. 2014, 2015, and 2020 land cover classifications achieved an overall accuracy of 90%, 92%, and 89%, respectively. The 2014 and 2015 land cover classifications had a Cohen's kappa accuracy higher than 0.90, but the 2020 land cover classification was slightly lower at 0.89. Every land cover class in each classified image achieved at least 85% in the user's accuracy and the producer's accuracy. Land cover

Table 2 Error matrix of land cover classification on Landsat 8 OLI/ TIRS (a) Year 2014 (b) Year 2015 and (c) Sentinel-2A image Year 2020

(a) 2014							
	Land Cover	**Vegetation**	**Barren land**	**River water**	**River Bar**	**Total**	**User's accuracy**
Classification	Vegetation	44	5	1		50	88.00
	Barren land	3	46		1	50	92.00
	River water		1	49		50	98.00
	River bar		1	3	46	50	92.00
	Total	47	53	53	47	200	
	Producer's accuracy (%)	93.62	86.79	92.45	97.87		
	Total accuracy (%)	92.50					
	Kappa accuracy	0.90					
(b) 2015							
	Land Cover	Vegetation	Barren land	River water	River Bar	Total	User's accuracy
Classifica-tion	Vegetation	49	1			50	98.00
	Barren land	2	44	3	1	50	88.00
	River water		2	48		50	96.00
	River bar		2	1	47	50	94.00
	Total	51	49	52	48	200	
	Producer's accuracy (%)	96.08	89.80	92.31	97.92		
	Total accuracy (%)	94.00					
	Kappa accuracy	0.92					
(c) 2020							
	Land Cover	Vegetation	Barren land	River water	River Bar	Total	User's accuracy
Classifica-tion	Vegetation	45	4	1		50	90.00
	Barren land		47	3		50	94.00
	River water		3	47		50	94.00
	River bar	1		4	45	50	90.00
	Total	46	54	55	45	200	
	Producer's accuracy (%)	97.83	87.04	85.45	100		
	Total accuracy (%)	92.00					
	Kappa accuracy	0.89					

classification pairs of consecutive years were cross-tabulated to investigate land cover changes from 2014 to 2015 (immediate impact) and 2015 to 2020 (five-year impact).

Land cover changes in the riparian zones

Figure 6 shows land cover changes in the riparian zones of the five rivers for the immediate impacts and the five-year impacts. The earthquake in riparian areas was devastating for the immediate impacts, as shown by a drastic increase in the river bar area, especially for the Penataran and Kadamaian Rivers. The increase of river bars at the Penataran River riparian zone was the highest among the five rivers, from 0 ha to 54.36 ha, whereas the Kadamaian River had an increase of 56.97 ha, from 35.82 ha (2014) to 92.79 ha (2015). The river bar areas only increased slightly in the other three rivers, at 1.08 ha, 1.44 ha, and 2.43 ha for the Wariu River, Tohubang River, and Kilambun River, respectively. The river with the highest increase in water area during the one-year change period is the Kilambun River (30.33 ha), followed by the Penataran River (19.26 ha) and the Kadamaian River (6.03 ha). Figure 6 also showed that both the Wariu and Tohubang rivers had a decrease in water area of 5.85 ha (3.6%) and 4.23 ha (13.28%), respectively. In addition, the barren land in the Kadamaian River showed the most significant decline of 25.35% (33.3 ha), followed by the Wariu River (9.51% or 22.5 ha). Meanwhile, in the 2014–2015 change period, Penataran River showed the slightest decrease in barren land of 3.06 ha, while having the highest loss in vegetation area of 69.21 ha, followed by Kilambun River (39.24 ha), Kadamaian River (29.43 ha) and Tohubang River (5.58 ha).

For the five-year impact, all rivers showed a decrease in river water area. Kilambun River showed the highest decrease in the river water class area by losing 26.05%, from 64.26 ha (2015) to 47.52 ha (2020). It was followed by the Penataran River (-22%), the Wariu River (-21.93%), the Kadamaian River (-18.77%), and lastly, the Tohubang River (-15.64%). For barren land, the Kilambun River and Penataran River increased by 3.06 ha and 10.44 ha, respectively. Vegetation area increased in all riparian areas, with the highest increase in the Kadamaian riparian area (108.18 ha), followed by Wariu (32.31 ha), Penataran (26.19 ha), Kilambun (12.42 ha), and Tohubang (11.52 ha) riparian areas. During these five years, rock, gravel, and sand deposition at the Penataran river bars

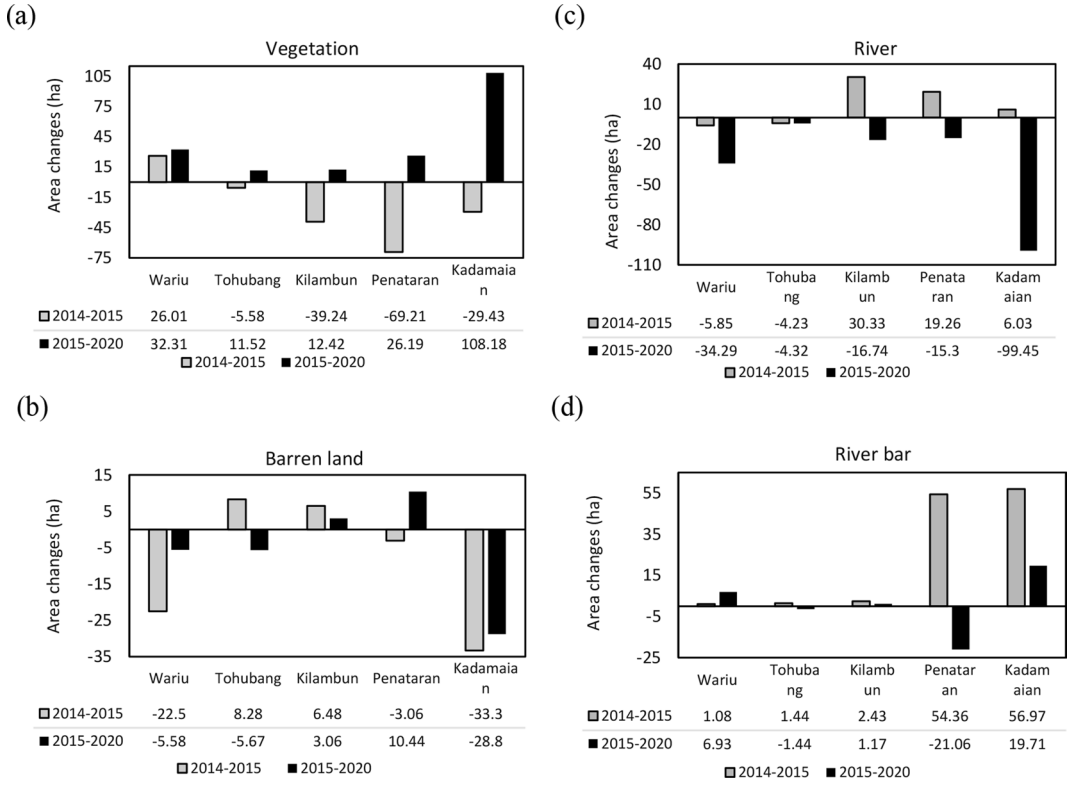

Fig. 6 Land cover changes in the riparian zones

decreased by 38.74%, from 54.36 ha (2015) to 33.3 ha (2020). Kadamaian River's bar area expanded another 19.71 ha to 112.23 ha in 2020. We focused on river bar changes in the Kadamaian and Penataran rivers, the two most affected rivers, for further land cover transition analysis.

Figure 7; Table 3 show the land cover transition from other land cover classes to river bars for the immediate impact period (2014–2015) and from river bars to other classes in the five-year post-earthquake period (2015–2020) for the Kadamaian River. 14.4 ha of the 35.82 ha of the bar area in 2014 remained unchanged. So, only 78.39 ha of the river bar area in 2015 was newly formed. These new river bars were vegetation, barren land, and river water before the earthquake. The transition of barren land into bars was the highest, with an area of 28.89 ha, followed by river water class (27.18 ha) and vegetation (22.32 ha). Five years after the earthquake, most of the river bars in 2015 had changed to other land cover types; 20.25 ha became barren land, 21.96 ha had transitioned to river water, and 25.65 ha were covered by vegetation. Only about 26.87% of the river bars (24.93 ha) of the Kadamaian River remained unchanged.

For the Penataran River (see Fig. 8), 54.36 ha of land was replaced by river bars in the immediate impact period, and only 16.2 ha of bars remained unchanged in the five-year post-earthquake period. For the immediate impact, vegetation was the largest area transitioning to river bars (22.05 ha), followed by barren land (21.60 ha) and river water (10.71 ha). In 2020, there were 33.9 ha of river bars, which consisted of 16.20 ha from 2015 and newly formed river bars of 17.7 ha Table 4.

Discussion

Multi-temporal remote sensing data is instrumental in mapping and analyzing post-earthquake land cover changes (Aydöner and Maktav 2009; Balamurugan and Aravind 2015; Fichera et al. 2012; Gong et al. 2012; Iwasaki et al. 2020; Jelének et al. 2018). However, analyzing land cover changes using multitemporal optical satellite imageries in the tropics is challenging due to the cloud cover problem. We used many satellite imageries from the same year to fill in the masked-out areas of cloud and the induced shadows, but some parts of the mountain areas were still affected by the problem. Nevertheless, our study only dealt with the riparian area impacted by the 2015 Ranau earthquake. We classified Landsat and Sentinel-2 imageries before and after the earthquake using OBIA because of its superior performance over the conventional pixel-based classification approach (Phua and Tsuyuki 2021; Ye et al. 2018). Image segmentation is typically a trial-and-error process of testing different shape, compactness, and scale parameter values (Clark et al. 2022). Generally, the values of these parameters

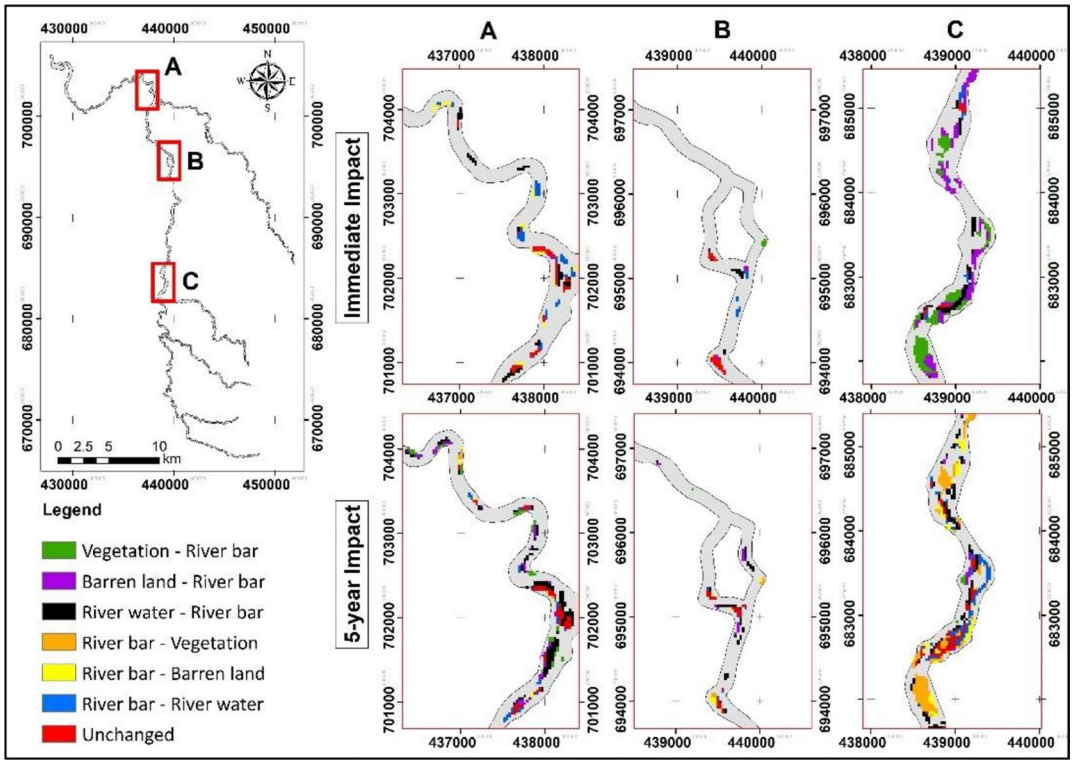

Fig. 7 Land cover transition of river bars in the Kadamaian River during one-year and five-year change periods

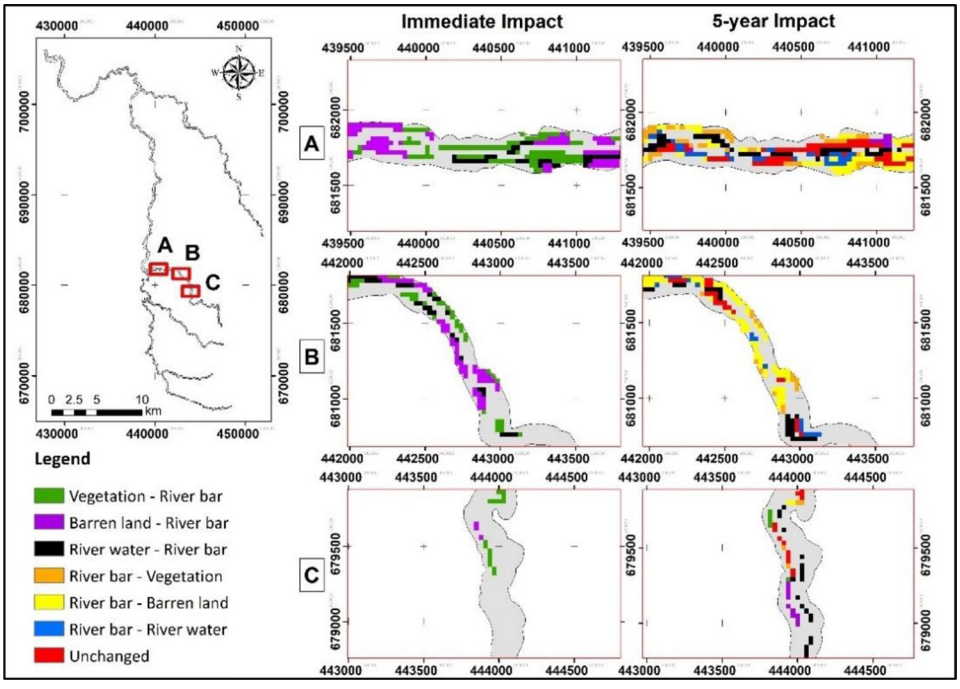

Fig. 8 Land cover transition of river bars in the Penataran River during one-year and five-year change periods

vary across imaging sensors, resolution, and application (Blaschke 2010). The segmentation parameters' values of the 2015 Landsat 8 imagery were usable for the 2016 imagery but were not applicable to the Sentinel imagery. The parameter's transferability is greatly affected by the sensor's radiometric resolution (Cánovas-García and Alonso-Sarría 2015) and spatial resolution (Clark et al. 2022); lower-resolution satellite imageries tend to have

Table 3 Land cover transition of river bars in the Kadamaian River during one-year and five-year change periods

One-year changes			Five-year changes		
From	**To**	**Area (ha)**	**From**	**To**	**Area (ha)**
Vegetation	River bars	22.32	River bars	Vegetation	25.65
Barren land		28.89		Barren land	20.25
River water		27.18		River water	21.96
				River bars	24.93
TOTAL		78.39 ha	TOTAL		92.79 ha
			Vegetation	River bars	7.47
			Barren land		17.55
			River water		62.28
			TOTAL		87.30 ha

Table 4 Land cover transition of river bars in the Penataran River during one-year and five-year change periods

One-year changes			Five-year changes		
From	**To**	**Area (ha)**	**From**	**To**	**Area (ha)**
Vegetation	River bars	22.05	River bars	Vegetation	8.91
Barren land		21.60		Barren land	20.34
River water		10.71		River water	8.91
				River bars	16.20
TOTAL		54.36 ha	TOTAL		54.36 ha
			Vegetation	River bars	0.63
			Barren land		2.07
			River water		14.4
			TOTAL		17.7 ha

higher segmentation scales. However, the classification accuracy of the Sentinel imagery in this study was only slightly different compared to the Landsat imageries.

There were more than 120 aftershocks with a magnitude above two during the three months after the mainshock on June 5, 2015 (Tongkul 2016). The aftershocks are confined to a narrow zone, and the aftershocks' depth gradually increases up to 30 km in the northwest direction. These earthquake-induced shocks cause massive landslides, especially in hillsides, mountain areas, and riverbanks within a water catchment (Xue et al. 2013). Removal of natural vegetation cover during mass movement is one of the critical factors that could significantly impact the geomorphology and hydrological functioning of a water catchment. Direct runoff increases when impermeable surfaces replace vegetation. It also leads to increased soil erosion and sediment transport that accumulate at the base of steep hillslopes, thus increasing the likelihood of debris flow occurring in due time (Simon et al. 2015). Among the five rivers, it was reported that the earthquake most impacted the Penataran River. It was noted that several hundred hectares of vegetation disappeared along with soil and rocks due to the landslides (Tongkul 2016). Our land cover change analyses revealed that vegetation decreased in the riparian areas of all rivers, except for the Wariu River, during the immediate impact period. The vegetation cover of the Penataran riparian area decreased the most among the five rivers. Deforestation in the Penataran riparian area was 1.76 and 2.35 times higher than in the Kilambun and Kadamaian rivers, respectively. Generally, earthquake-induced landslides trigger severe erosion in the hills and mountains, leading to soil degradation. As expected, soil erosion and landslides increased in years following the earthquake due to the absence of vegetation that affords rainfall interception and soil-binding processes. This high erosion rate may accelerate topsoil loss and further prevent revegetation (Roslee et al. 2018), thus entering a positive feedback mechanism until equilibrium is achieved. However, increased vegetation cover was observed predominantly in Kadamaian and Panataran riparian areas in the five-year impact period. The vegetation cover increase in the Kadamaian riparian area was 4.13 times that of the Penataran riparian area.

Besides erosion, deposition is a critical factor affecting the accumulation of sediment layers in river channels over time. These disturbances have a clear correlation with debris flow in a water catchment. Debris flow occurs when soil and rock materials are loosened, and water is saturated. When this occurs in steep mountainous areas, gravity can mobilize soil and rocks rapidly downhill (Edgar et al. 2018). Deposition in river channels downstream occurs when streamflow slows down, causing sediment and debris to accumulate along the rivers as river bars (Roslee and Norhisham 2018). These sediments can vary in composition, ranging from fine-grained materials such as sand and silt to larger rocks and boulders (Roslee and Sharir 2019).

The object-based classifications captured the formation of river bars in the study area. Based on the land cover time series, single "forced bars" were the primary bar type observed in the study area. Point bars, which form inside a river bend, and central bars, which form in more comprehensive sections, are examples of forced bars. As a mixture of loose materials forms the river bars, the river channels in the study area have been experiencing changes over time. Through object-based image analysis, we found that the changes in river bars in the Kadamaian and Penataran rivers were the highest among the five rivers. The river bar areas increased on both rivers in the one-year change period. The river bar increased more than 2.5 times to 92.79 ha in 2015 for the Kadamaian River. The Penataran River had no river bar before the earthquake, but new river bar areas of 54.36 ha were formed a year later. The river bar area in the Kadamaian River further increased to 112.23 ha in 2020. In contrast, the Penataran River experienced a decrease in river bar area to 33.3 ha in the five-year change period.

Although the riparian area of the Penataran River is five times smaller than that of the Kadamaian River, the river bar cover rate of the Penataran River after the earthquake is higher than that of the Kadamaian River. The river bar cover in the Panataran riparian area was 20.59%, compared to only 6.83% for the Kadamaian riparian area in 2015. In 2020, the river bar cover was 12.61% and 8.28% for Penataran and Kadamaian riparian areas, respectively. Considering that the Penataran River is an order lower than the Kadamaian River, the governing influence of stream order associated with a steeper gradient and smaller catchment size could have overridden other factors such as land cover, soil, and lithology (Clarke and Walsh 2006; Grieve et al. 2018; Shaw and Cooper 2008). The sediments in the Panataran River are odd to be transported to the Kadamaian River since the upper parts of the catchment have steeper gradients, which facilitate debris movement by the effect of gravity (Nainar et al. 2018; Pike and Scatena 2010).

Further analysis by breaking up the Kadamaian River into two sections: Kadamaian Upper (before the Penataran confluence) and Kadamaian Lower (after the Penataran confluence) revealed that the loss in river bar areas in the Penataran and Kadamaian Upper rivers corresponds to a gain in the Kadamaian Lower River. This may reflect the dynamic nature of these river systems and imply that bedload mobilization was still active up to five years post-earthquake (2015–2020). Besides material mobilization within the channel, it is also possible that other deposition mechanisms, namely material mobilization from the catchment side slope to the river channel, may have contributed to the changes in the river bars (Chappell et al. 2004). This can only be ascertained with further geochemical or geophysical investigation in the future (Sugumaran et al. 2023). At present, our aim is not to balance the sediment budget but to demonstrate the extent of bedload mobilization following an earthquake.

Based on the land cover changes in the immediate and five-year impact periods, it is evident that the earthquake most impacted the Penataran River and Kadamaian River. The formation of river bars was one of the most important causes of river channel changes in the study area. Thus, detailed land cover transitions to and from river bars in the two most affected rivers were analyzed based on the land cover time series. The earthquake caused a significant increase in river bars in the Kadamaian River. Of the 78.39 ha of new river bars in 2015, 34.67% were river water areas before the earthquake. For the Panataran River, almost 20% of the newly deposited river bars (54.36 ha) were river water areas before the earthquake. The transition from river water to river bar continued to occur during the five-year change period. The new river bar areas that originated from river water areas between 2015 and 2020 were 71.12% and 81.36% for the Kadamaian River and Panataran River, respectively. These findings indicate the reduction of river channel area, thus altering water flow patterns in the earthquake-affected rivers. The sediment accumulation in river bars also leads to raised riverbeds. This eventually causes a reduction in channel capacity and an alteration in water flow patterns, increasing the risk of flooding, especially during heavy rainfall (Bohorquez and del Moral-Erencia JD 2017; Mahmood et al. 2022).

The spatial resolution of the Landsat and Sentinel imageries might limit the impact of the earthquake derived from the multitemporal satellite imageries. For instance, river bars smaller than the pixel's size are likely undetected. Moreover, river water areas may vary due to rainfall variations in different acquisition times of the imageries. The five-year change period included mild El Niño (2018–2019) and La Niña (mild, 2016–2018; moderate, 2020) phases. Since bedload mobilisation and mass movements are directly proportionate to rainfall amount and intensity, the magnitude and frequency of change could be higher than that observed in this study in stronger La Niña years, especially with the increased rainfall brought about by climate change. Overall, the findings from the object-based land cover change analyses have contributed significantly to better disaster management in Sabah. By mapping the post-earthquake land cover changes, this study provided essential data for assessing the extent of the impacts and identifying the areas that required mitigation actions. Moreover, the insights gained in this study guide long-term planning and policy-making for the conservation of resilient river systems after seismic disturbances.

Conclusion

Earthquakes cause devastating impacts on the river systems in a catchment. Based on the object-based classification of multi-temporal satellite imageries, we assessed the 2015 Ranau earthquake-induced land cover changes in the riparian areas of the affected rivers. The five rivers in the catchment were affected to varying degrees. The Panataran River and Kadamaian River were most affected regarding vegetation loss and river bar formation. Detailed land cover transitions to and from river bars revealed the significant loss of river water areas in these two most affected rivers in the immediate impact period. However, the responses of river systems of different orders, sizes, and gradients were different in the five-year impact period. The river bar area in the Panataran River, which is smaller and lower order, decreased over the five years. In contrast, the river bar in the Kadamaian River, the larger and higher-order river, continued to increase during the period. By tracking land cover transition over time, it is possible to identify channel alteration due to river bar formation and predict areas vulnerable

to flooding in the future. Further studies in post-earthquake vegetation recovery and improving the land cover mapping using high-resolution remote sensing imageries, including UAS imageries, are recommended. Deep learning models with OBIA in the high-resolution land cover mapping should be investigated to enhance the land cover analysis for post-disaster impact assessment. The land cover change information can be used to design appropriate flood mitigation measures and plan adaptive land management for ecosystem restoration in Sabah and other earthquake-affected areas.

Acknowledgements
The authors would like to thank the generous assistance and cooperation of various parties involved in this study. We are also thankful to editor and anonymous reviewers who provided valuable comments and suggestions for the improvement of the manuscript.

Author contributions
MHP: Conceptualization, Supervision, LTC, WVCW: Data curation, Validation, RR, AN, LTC, WVCW: Investigation, LTC: Data analysis, Visualization, Writing- Original draft preparation. MHP, WVCW: Methodology, Software, RR, AN, MHP: Writing-Reviewing and Editing. All authors have read and agreed to the published version of the manuscript.

Funding
This research was funded by Universiti Malaysia Sabah through Skim Dana Nic (DN20080) and Skim Dana Khas (SDK0295-2020).

Data availability
Data and materials are available upon request.

Declarations

Ethics approval and consent to participate
Not applicable.

Competing interests
The authors declare no competing interests.

Received: 17 July 2023 / Accepted: 17 April 2024
Published online: 15 May 2024

References

Adnan A, Harith N (2017) Estimation of peak ground acceleration of Ranau based on recent earthquake databases. MJG 1(2):6–9
Aguilar MA, Nemmaoui A, Novelli A, Aguilar FJ, García Lorca A (2016) Object-based greenhouse mapping using very high resolution satellite data and landsat 8 time series. Remote Sens 8(6):513. https://doi.org/10.3390/rs8060513
Ansari EM, Caldera HJ, Heshami S, Moshahedi N, Wirasinghe SC (2016) The severity of earthquake events—statistical analysis and classification. Int J Urban Sc 20:4–24. https://doi.org/10.1080/12265934.2016.1138876
Aydöner C, Maktav D (2009) The role of the integration of remote sensing and GIS in land use/land cover analysis after an earthquake. Int J Remote Sens 30(7):1697–1717. https://doi.org/10.1080/01431160802642289
Azeez OS, Shafri HZ, Alias AH, Haron NA (2022) Integration of Object-Based Image Analysis and Convolutional Neural Network for the classification of high-Resolution Satellite Image: a comparative Assessment. Appl Sci 27 12(21):10890. https://doi.org/10.3390/app122110890
Balamurugan G, Aravind MJ (2015) Land use land cover changes in pre-and post-earthquake affected area using Geoinformatics–Western Coast of Gujarat, India. Disaster Adv 8(4):1–14
Basharat M, Riaz MT, Jan MQ, Xu C, Riaz S (2021) A review of landslides related to the 2005 Kashmir Earthquake: implication and future challenges. Nat Hazards 108:1–30. https://doi.org/10.1007/s11069-021-04688-8
Blaschke T (2010) Object based image analysis for remote sensing. ISPRS J Photogramm Remote Sens 65(1):2–16. https://doi.org/10.1016/j.isprsjprs.2009.06.004
Bohorquez P, del Moral-Erencia JD (2017) 100 years of competition between reduction in channel capacity and streamflow during floods in the Guadalquivir River (Southern Spain). Remote Sens 9(7):727. https://doi.org/10.3390/rs9070727
Cánovas-García F, Alonso-Sarría F (2015) A local approach to optimize the scale parameter in multiresolution segmentation for multispectral imagery. Geocarto Int 30(8):937–961. https://doi.org/10.1080/10106049.2015.1004131
Chappell NA, Douglas I, Hanapi JM, Tych W (2004) Sources of suspended sediment within a tropical catchment recovering from selective logging. Hydrol Process 18(4):685–701. https://doi.org/10.1002/hyp.1263
Clark A, Moorman B, Whalen D, Vieira G (2022) Multiscale object-based classification and feature extraction along Arctic coasts. Remote Sens 14(13):2982. https://doi.org/10.3390/rs14132982
Clarke MA, Walsh RP (2006) Long-term erosion and surface roughness change of rain-forest terrain following selective logging, Danum Valley, Sabah, Malaysia. CATENA 68(2–3):109–123. https://doi.org/10.1016/j.catena.2006.04.002
Croissant T, Steer P, Lague D, Davy P, Jeandet L, Hilton RG (2019) Seismic cycles, earthquakes, landslides and sediment fluxes: linking tectonics to surface processes using a reduced-complexity model. Geomorphology 339:87–103. https://doi.org/10.1016/j.geomorph.2019.04.017
Edgar J Jr, Tongkul F, Roslee R (2018) Debris Flow Susceptibility Assessment at A Basin Scale: A Case Study at Bundu Tuhan, Ranau, Sabah, Malaysia. ASM Sci J 11: Special Issue 2018 (2) for SANREM (Natural Resources) 36–48
Fan X, Nie G, Deng Y, An J, Zhou J, Xia C, Pang X (2019) Estimating earthquake-damage areas using Landsat-8 OLI surface reflectance data. Int J Disaster Risk Reduct 33:275–283. https://doi.org/10.1016/j.ijdrr.2018.10.013
Fichera CR, Modica G, Pollino M (2012) Land Cover classification and change-detection analysis using multi-temporal remote sensed imagery and landscape metrics. Eur J Remote Sens 45(1):1–18. https://doi.org/10.5721/EuJRS20124501
Gong J, Yue Y, Zhu J, Wen Y, Li Y, Zhou J, Wang D, Yu C (2012) Impacts of the Wenchuan Earthquake on the Chaping River upstream channel change. Int J Remote Sens 33(12):3907–3929. https://doi.org/10.1080/01431161.2011.636767
Grieve SW, Hales TC, Parker RN, Mudd SM, Clubb FJ (2018) Controls on zero-Order Basin morphology. J Geophys Res Earth Surf 123(12):3269–3291. https://doi.org/10.1029/2017JF004453
Guirado E, Blanco-Sacristan J, Rodriguez-Caballero E, Tabik S, Alcaraz-Segura D, Martinez-Valderrama J, Cabello J (2021) Mask R-CNN and OBIA fusion improves the segmentation of scattered vegetation in very high-resolution optical sensors. Sensors 21(1):320. https://doi.org/10.3390/s21010320
Ishihara M, Tadono T (2017) Land cover changes induced by the great east Japan earthquake in 2011. Sci Rep 7(1):45769. https://doi.org/10.1038/srep45769
Iwasaki Y, Tamaki T, Murata K, Koga A, Fujimoto K (2020) Detection of land cover changes before and after the 2016 Kumamoto earthquake in Japan using remote sensing for evaluation of environmental impacts. InIOP Conference Series: Earth and Environmental Science 2020 Nov 1 (Vol. 581, No. 1, p. 012044). IOP Publishing. https://doi.org/10.1088/1755-1315/581/1/012044
Jelének J, Kopačková V, Fárová K (2018) Post-earthquake landslide distribution assessment using sentinel-1 and-2 data: The example of the 2016 mw 7.8 earthquake in New Zealand. InProceedings 2018 Mar 22 (Vol. 60, No. 1). MDPI. https://doi.org/10.3390/ecrs-2-05174
Kamlisa UK, Bürger-Arndt R (2016) A conceptual framework approach on mapping multiple ecosystem services in tropical wetland areas on a local scale. Asia-Pac J Innov Hosp Tour 5(3):183–202
Li M, Ma L, Blaschke T, Cheng L, Tiede D (2016) A systematic comparison of different object-based classification techniques using high spatial resolution imagery in agricultural environments. Int J Appl Earth Obs Geoinf 49:87–98. https://doi.org/10.1016/j.jag.2016.01.011
Liu D, Xia F (2010) Assessing object-based classification: advantages and limitations. Remote Sens Lett 1(4):187–194. https://doi.org/10.1080/01431161003743173
Liu S, Qi Z, Li X, Yeh AG (2019) Integration of convolutional neural networks and object-based post-classification refinement for land use and land cover mapping with optical and SAR data. Remote Sens 11(6):690. https://doi.org/10.3390/rs11060690
Liu T, Yang L, Lunga D (2021) Change detection using deep learning approach with object-based image analysis. Remote Sens Environ 256:112308. https://doi.org/10.1016/j.rse.2021.112308

Mahmood I, Qureshi SN, Tariq S, Atique L, Iqbal MF (2015) Analysis of landslides triggered by October 2005, Kashmir Earthquake. PLoS Curr 7. https://doi.org/10.1371%2Fcurrents.dis.0bc3ebc5b8adf5c7fe9fd3d702d44a99

Mahmood A, Han JC, Ijaz MW, Siyal AA, Ahmad M, Yousaf M (2022) Impact of sediment deposition on Flood carrying capacity of an Alluvial Channel: a case study of the Lower Indus Basin. Water 14(20):3321. https://doi.org/10.3390/w14203321

Nainar A, Bidin K, Walsh RP, Ewers RM, Reynolds G (2017) Effects of different land-use on suspended sediment dynamics in Sabah (Malaysian Borneo)–a view at the event and annual timescales. Hydrol Res Lett 11(1):79–84. https://doi.org/10.3178/hrl.11.79

Nainar A, Tanaka N, Bidin K, Annammala KV, Ewers RM, Reynolds G, Walsh RP (2018) Hydrological dynamics of tropical streams on a gradient of land-use disturbance and recovery: a multi-catchment experiment. J Hydrol 566:581–594. https://doi.org/10.1016/j.jhydrol.2018.09.022

Phiri D, Morgenroth J (2017) Developments in Landsat land cover classification methods: a review. Remote Sens 9(9):967. https://doi.org/10.3390/rs9090967

Phua MH, Tsuyuki S (2021) Assessing impact of multiple fires on a Tropical Peat Swamp Forest using high and very high-Resolution Satellite images. Fire 4(4):89. https://doi.org/10.3390/fire4040089

Phua MH, Tsuyuki S, Lee JS, Sasakawa H (2007) Detection of burned peat swamp forest in a heterogeneous tropical landscape: a case study of the Klias Peninsula, Sabah, Malaysia. Landsc Urban Plan 82(3):103–116. https://doi.org/10.1016/j.landurbplan.2007.01.021

Pike AS, Scatena FN (2010) Riparian indicators of flow frequency in a tropical montane stream network. J Hydrol 382(1–4):72–87. https://doi.org/10.1016/j.jhydrol.2009.12.019

Rojas C, Mauricio V, Sergio O, Peters S, Constanza V (2013) Pre and post earthquake land use and land cover identification in Concepción. Earth Observation of Global Changes (EOGC). Springer, Berlin, Heidelberg, pp 223–231. https://doi.org/10.1007/978-3-642-32714-8_15.

Roslee R, Norhisham MN (2018) Flood susceptibility analysis using multi-criteria evaluation model: a case study in Kota Kinabalu, Sabah. ASM Sci J 11:123–123

Roslee R, Sharir K (2019) Integration of GIS-Based RUSLE model for land planning and environmental management in Ranau Area, Sabah, Malaysia. ASM Sc J 12(3):60–69

Roslee R, Tongkul F, Mariappan S, Simon N (2018) Flood hazard analysis (FHAn) using multi-criteria evaluation (MCE) in Penampang Area, Sabah Malaysia. ASM Sci J 11(3):104–122

Rosli MI, Che Ros F, Razak KA, Ambran S, Kamaruddin SA, Nor Anuar A, Marto A, Tobita T, Ono Y (2021) Modelling debris flow runout: a case study on the Mesilau Watershed, Kundasang, Sabah. Water 13(19):2667. https://doi.org/10.3390/w13192667

Sharir K, Lai GT, Simon N, Ern LK, Madran E, Roslee R (2022) Debris flow susceptibility analysis using a bivariate statistical analysis in the Panataran River, Kg Melangkap, Sabah, Malaysia. InIOP Conference Series: Earth and Environmental Science 2022 Nov 1 (Vol. 1103, No. 1, p. 012038). IOP Publishing

Shaw JR, Cooper DJ (2008) Linkages among watersheds, stream reaches, and riparian vegetation in dryland ephemeral stream networks. J Hydrol 350(1–2):68–82. https://doi.org/10.1016/j.jhydrol.2007.11.030

Sidle RC, Ziegler AD, Negishi JN, Nik AR, Siew R, Turkelboom F (2006) Erosion processes in steep terrain—Truths, myths, and uncertainties related to forest management in Southeast Asia. Ecol Manag 224(1–2):199–225. https://doi.org/10.1016/j.foreco.2005.12.019

Simon N, Crozier M, de Roiste M, Rafek AG, Roslee R (2015) Time Series Assessment on Landslide Occurrencs in an Area Undergoing Development. Singap J Trop Geogr 36(1):98–111. https://doi.org/10.1111/sjtg.12096

Sugumaran D, Blake WH, Millward GE, Yusop Z, Mohd Yusoff AR, Mohamad NA, Nainar A, Annammala KV (2023) Composition of deposited sediment and its temporal variation in a disturbed tropical catchment in the Kelantan river basin, Peninsular Malaysia. Environ Sci Pollut Res 11:1–16. https://doi.org/10.1007/s11356-022-19904-6

Timilsina S, Aryal J, Kirkpatrick JB (2020) Mapping urban tree cover changes using object-based convolution neural network (OB-CNN). Remote Sens 12(18):3017. https://doi.org/10.3390/rs12183017

Tjia HD (1978) The Lahad Datu (Sabah) earthquake of 1976: surface deformation in the epicentral region. Sains Malays 7:33–64

Tjia HD (2007) Kundasang (Sabah) at the intersection of regional fault zones of quaternary age. Bull Geol Soc Malaysia 53:59–66

Tongkul F (1989) Recent strike-slip fault movement associated with a mud volcano in the Lahad Datu area, Sabah. Sains Malays 18(1):23–31

Tongkul F (2016) The 2015 Ranau Earthquake: cause and impact. Sabah Soc J 32:1–28

Tongkul F (2017) Active tectonics in Sabah – seismicity and active faults. Bull Geol Soc Malaysia 64:27–36

Tongkul F (2021) An overview of earthquake science in Malaysia. ASM Sci 14:1–12. https://doi.org/10.32802/asmscj.2020.440

Vali A, Comai S, Matteucci M (2020) Deep learning for land use and land cover classification based on hyperspectral and multispectral earth observation data: a review. Remote Sens 12(15):2495. https://doi.org/10.3390/rs12152495

Wang Y, Wei S, Wang X, Lindsey EO, Tongkul F, Tapponnier P, Bradley K, Chan CH, Hill EM, Sieh K (2017) The 2015 M w 6.0 Mt. Kinabalu earthquake: an infrequent fault rupture within the Crocker fault system of East Malaysia. Geosci Lett 4(1):1–12. https://doi.org/10.1186/s40562-017-0072-9

Wang J, Wang Z, Cheng H, Kang J, Liu X (2022) Land cover changing pattern in pre-and post-earthquake affected area from Remote Sensing Data: a case of Lushan County, Sichuan Province. Land 11(8):1205. https://doi.org/10.3390/land11081205

World Weather Information Service (2014) – Kota Kinabalu https://web.archive.org/web/20131023025934/http://worldweather.wmo.int/020/c00081.htm. (Accessed 11

Wright NG, Crosato A (2011) The hydrodynamics and morphodynamics of rivers. In Treatise on Water Science; Elsevier Science Ltd. https://doi.org/10.1016/B978-0-444-53199-5.00033-6

Xue L, Xiaoli L, Jinggang L, Lifen Z, Qiuliang W, Wulin L (2013) Correlation between seismicity and geomorphology in Dingxi Basin, Gansu Province, China. Geod Geodyn 4(4):17–25. https://doi.org/10.3724/SP.J.1246.2013.04017

Ye S, Pontius RG Jr, Rakshit R (2018) A review of accuracy assessment for object-based image analysis: from per-pixel to per-polygon approaches. ISPRS J Photogramm Remote Sens 141:137–147. https://doi.org/10.1016/j.isprsjprs.2018.04.002

Yu W, Zhou W, Qian Y, Yan J (2016) A new approach for land cover classification and change analysis: integrating backdating and an object-based method. Remote Sens Environ 177:37–47. https://doi.org/10.1016/j.rse.2016.02.030

Zhou W, Troy A, Grove M (2008) Object-based land cover classification and change analysis in the Baltimore metropolitan area using multitemporal high resolution remote sensing data. Sensors 8(3):1613–1636. https://doi.org/10.3390/s8031613

Publisher's Note